Towards photocatalytic water splitting in homogeneous solutions using molecular metalloporphyrin photosensitizers and catalysts

Liu, C.

3

Effects of Electron-Withdrawing and Electron-Donating Substituents on the pH Dependence of Co(III)-porphyrin Catalysts for Homogeneous Photocatalytic Hydrogen Evolution

A series of anionic Co(III)- and Zn(II)-porphyrin complexes bearing either electron-donating ($[M\text{-}OMeP]^{n-}$, $[M\text{-}MeP]^{n-}$, M = Co, n =3 or M = Zn, n = 4) or electron-withdrawing ($[M\text{-}F8P]^{n-}$, $[M\text{-}F16P]^{n-}$) substituents were prepared to study the role of electronic effects on homogeneous photocatalytic hydrogen evolution in presence of $[Ru(bpy)_3]^{2+}$ as photosensitizer (PS), blue light irradiation (450 nm), and ascorbate and tris(2-carboxyethyl)phosphine hydrochloride (TCEP) as sacrificial electron donor. Electronic effects not only controlled the redox properties of the metal-porphyrin catalysts, they also changed the photocatalytic hydrogen evolution mechanism. Electrochemical studies and kinetic studies in photocatalytic conditions indicated that the two best catalysts, i.e., the electron-rich $[Co\text{-}OMeP]^{3-}$ and electron-poor $[Co\text{-}F16P]^{3-}$ compounds, catalyzed the hydrogen evolution reaction (HER) via two different mechanisms: one centered on the metal for $[Co\text{-}OMeP]^{3-}$, whereas for $[Co\text{-}F16P]^{3-}$ HER catalysis more likely proceeds via a mechanism involving both the metal center and the porphyrin ligand. Strikingly, the pH dependence of the photocatalytic activity of these two catalysts was found to be very different. For $[Co\text{-}F16P]^{3-}$ the highest activity and stability was observed at pH 7.0, with a maximum TOF of 6.7 ± 0.3 h^{-1} and a TON of 70 ± 3 after 39.5 hours of irradiation, while $[Co\text{-}OMe]^{3-}$ performed more classically, with better performances at pH 4.1: in such conditions the maximum TOF was 7.2 ± 0.4 h^{-1} and the TON 175 ± 5 after 39.5 h irradiation. In this family of hydrogen-evolution catalysts, it is hence preferable to functionalize the complex with electron-withdrawing groups to maximize photocatalytic activity at neutral pH. With $[Co\text{-}F16P]^{3-}$ or $[Co\text{-}OMeP]^{3-}$ as catalyst, photocatalysis was limited by the PS decomposition.

3.1 Introduction

Light-induced H_2 evolution in aqueous solutions has generated great attention since it could contribute to providing a sustainable and environmentally friendly energy conversion system.[1] In order to drive this photoreaction efficiently, well-performing hydrogen-evolving catalysts (HECs) must be prepared, the design of which is not yet fully understood.[2-4] Recently, studies on molecular hydrogen evolution catalysts have multiplied due to their numerous advantages: 1) they mimic the active sites of heterogeneous catalysts and allow to approach catalytic mechanisms with atomic precision;[5-7] 2) ligand functionalization allows for fine-tuning of the coordination sphere and electronic density of the metal center, which is a powerful tool to establish relationships between the properties of the metal center and its photocatalytic performances;[7,8] and 3) they can be integrated in supramolecular water splitting systems, also in combination with solid-state materials and catalysts.[9-11]

In principle, a good molecular HEC should have three characteristics: 1) it should include a metal center that can switch between different oxidation states;[1] 2) it should be made with a ligand set that provides a stable coordination environment to the metal ion, especially for labile low-valent metal ions;[1,4] and 3) its electronic density should balance the reaction rates and over-potential of the different catalytic steps, to achieve the highest possible rate.[7,8] In the last decade, molecular HECs have been extensively studied for photocatalytic hydrogen evolution, especially those made of first-row transition metals.[12-28] Many of those catalysts are based on cobalt, which is available in large quantities on Earth and has more than five available oxidation states.[29,30] Usually, these catalysts show better catalytic properties in mildly acidic conditions (pH = 4-5), where enough protons are available for the fast generation of H_2. On the other hand, coupling proton reduction and water oxidation to achieve a full water splitting scheme, may be more favorable in neutral conditions, because water oxidation becomes very challenging at low pH. Still, examples of cobalt-based HECs working at pH 7.0 in homogeneous aqueous solutions are very rare.[31,32]

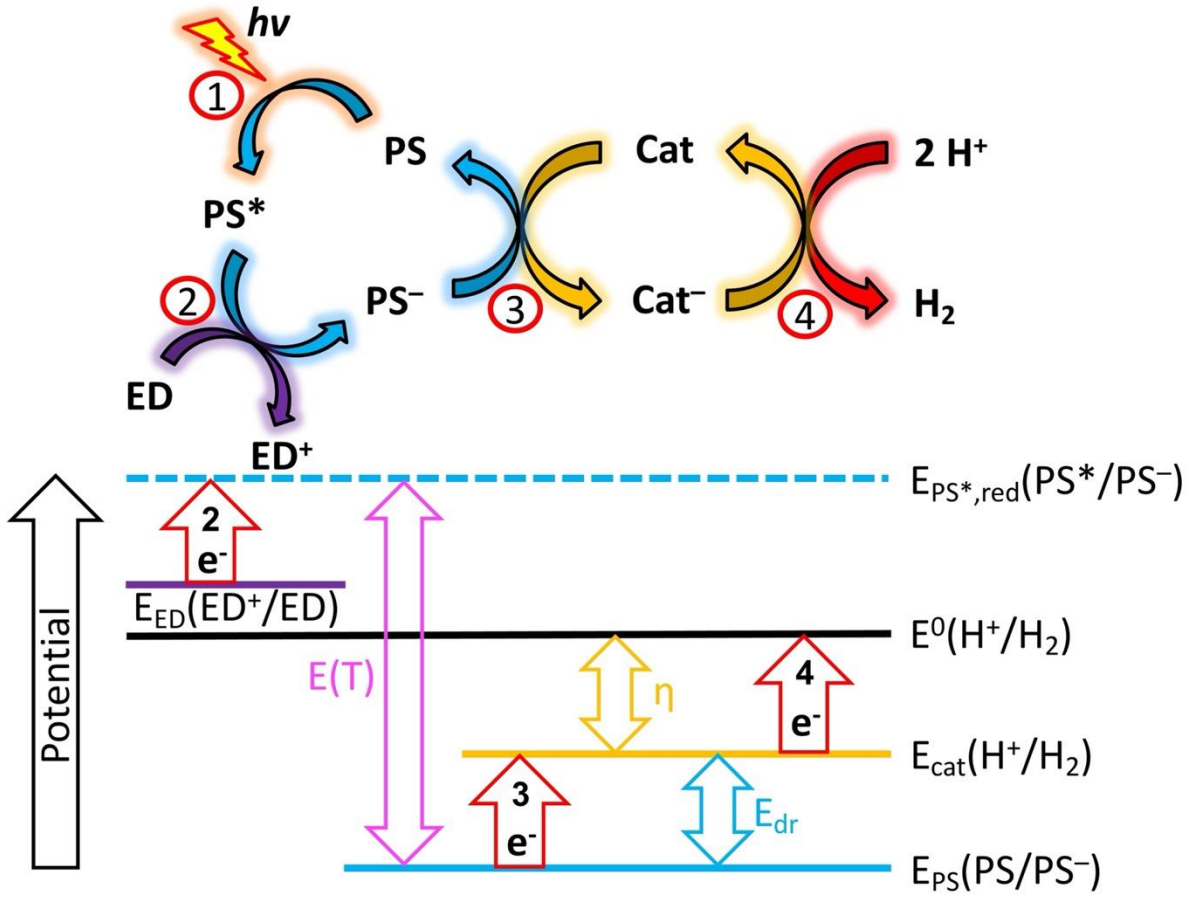

Figure 3.1 *Energy scheme and simplified photocatalytic mechanism of the reductive quenching pathway in a three-component molecular photocatalytic hydrogen-evolution system. ED: sacrificial electron donor; PS: photosensitizer; Cat: hydrogen evolution catalyst; E(T): triplet excited state energy of the PS; η: overpotential of the catalyst;* E_{dr}*: driving force of the electron-transfer step from the reduced photosensitizer* PS^- *to the catalyst.*

Photocatalytic H_2-evolving systems contain, next to the catalyst, a photosensitizer (PS) and a sacrificial electron donor (ED). In such 3-component systems the much higher concentration of the ED, compared to the catalyst (Cat), usually favors kinetically the excited state PS* to be quenched reductively by ED to afford PS^- (Step 2 in Figure 3.1).[4] PS^- then reduces Cat to Cat^- (Step 3), an electron-transfer step driven by the driving force E_{dr}. This process, when repeated twice, catalytically leads to the formation of an H_2 molecule (Step 4). In such a system a good balance between E_{dr} and the overpotential of the catalyst (η) is needed to keep both Step 3 and Step 4 fast enough.[8] Functionalization of the catalyst with electron-donating or electron-withdrawing groups in principle allows for optimization of E_{dr} and η. However, for synthetic reasons it is not always easy to vary systematically the redox properties of a cobalt complex to optimize its redox potential for catalytic hydrogen reduction. In addition, the pH dependence

of the highest activity of a cobalt catalyst (Step 4 in Figure 3.1) may also depend strongly on the electron-density on the metal catalyst. In the two studies where systematic ligand functionalization by electron-donating or -withdrawing groups has been realized,[19,33] the pH dependence of the activity of the HEC has not been investigated. In general, it remains poorly understood which influence electron-withdrawing or electron-donating groups have on the (photo)catalytic activity of HEC, and in particular on their pH dependence.

Porphyrin ligands offer stable and rigid coordination sites for cobalt ions, while being readily tunable with electron-donating or -withdrawing substituents, which makes them very attractive for the fine-tuning of molecular catalysts.[1,34,35] In this work, a family of water-soluble Co(III) porphyrin complexes was prepared bearing either electron-donating ([Co-OMeP]$^{3-}$, [Co-MeP]$^{3-}$) or electron-withdrawing ([Co-F8P]$^{3-}$, [Co-F16P]$^{3-}$) substituents (Figure 3.2). This series of compounds was used to investigate the effect of the electron-richness of the ligand on homogeneous photocatalytic hydrogen evolution in presence of $[Ru(bpy)_3]Cl_2$ as photosensitizer (PS), and ascorbic acid (AA) and tris(2-carboxyethyl)phosphine hydrochloride (TCEP) as sacrificial electron donor (ED).[12,36] The pH dependence of their (photo)catalytic properties was investigated and compared to those of their Zn^{2+} analogues, in which the metal center cannot accommodate any changes of the oxidation state. This study demonstrates that the cooperation of the ligand during HEC and the pH dependence of the catalyst both strongly depend on the electron-richness of the porphyrin ligand. Thus, we show that good catalysts can be obtained for the HER at pH 7, provided that the ligand is very electron-poor.

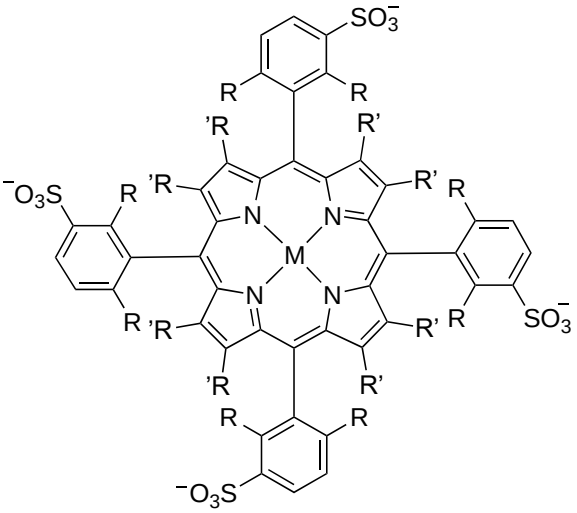

[Co-OMeP]$^{3-}$: M = Co^{III}, R = OCH_3, R' = H
[Co-MeP]$^{3-}$: M = Co^{III}, R = CH_3, R' = H
[Co-F8P]$^{3-}$: M = Co^{III}, R = F, R' = H
[Co-F16P]$^{3-}$: M = Co^{III}, R = F, R' = F
[Zn-OMeP]$^{4-}$: M = Zn^{II}, R = OCH_3, R' = H
[Zn-MeP]$^{4-}$: M = Zn^{II}, R = CH_3, R' = H
[Zn-F8P]$^{4-}$: M = Zn^{II}, R = F, R' = H
[Zn-F16P]$^{4-}$: M = Zn^{II}, R = F, R' = F
[H_2-OMeP]$^{4-}$: M = 2 H^+, R = OCH_3, R' = H
[H_2-MeP]$^{4-}$: M = 2 H^+, R = CH_3, R' = H
[H_2-F8P]$^{4-}$: M = 2 H^+, R = F, R' = H
[H_2-F16P]$^{4-}$: M = 2 H^+, R = F, R' = F

Figure 3.2 *Chemical structures of the water-soluble metal porphyrin complexes and free base ligands used in this work. All compounds were isolated as Na^+ salts.*

3.2 Results and Discussion

3.2.1 Synthesis

The tetra-sulfonated free-base porphyrin ligands $Na_4[H_2\text{-OMeP}]$,[8] $Na_4[H_2\text{-MeP}]$,[37] $Na_4[H_2\text{-F8P}]$,[38] $Na_4[H_2\text{-F16P}]$,[39] and their metal complexes $Na_4[Co\text{-F8P}]$,[40,41] $Na_4[Zn\text{-F8P}]$,[42] $Na_4[Zn\text{-F16P}]$,[39] were synthesized according to reported methods. The other Co(III) and Zn(II) porphyrin compounds described in this Chapter are new and were synthesized via refluxing the free-base ligands with Co(II) sulfate or Zn(II) dichloride in Milli-Q water for 12 h. Na^+-loaded ion exchange resin was used to exchange the counter ions with Na^+, and the complexes were finally purified by size-exclusion chromatography in order to remove all inorganic salts in excess. According to NMR all cobalt compounds are diamagnetic and hence contain low-spin Co(III) ions. The Co(III) porphyrin complexes were supposedly formed due to the oxidation of Co(II) by air during purification.[40,41,43] Full characterization is given in the Supplementary Information (Figure AII.1 - Figure AII.6).

3.2.2 Electrochemical properties

In principle, the electron-richness of a ligand influences the redox and electrocatalytic properties of its metal complex.[7,32] Another classical idea in hydrogen-evolution catalysis is that lower pH values render most catalysts more efficient at catalyzing the HER. The redox properties of the Co(III) and Zn(II) porphyrin complexes were hence studied with electrochemical methods at pH 7.0 and pH 4.1. Cyclic voltammetry (CV), linear sweep voltammetry (LSV), and differential pulse voltammetry (DPV), were recorded, using a phosphate buffer and a glassy-carbon (GC) working electrode (Figure 3.3). DPV of the four Co(III)-porphyrin complexes at pH 7.0, show that lowering of the electron-richness of the complex leads to a decrease of the potential of the first reduction wave that turns the Co(III)-porphyrins (Co^{III}-P) into Co(II)-porphyrins (Co^{II}-P). This reduction wave was observed at −0.53 V vs. NHE for the most electron-poor complex $[Co\text{-F16P}]^{3-}$, and at −0.75 V vs. NHE for the most electron-rich compound $[Co\text{-OMeP}]^{3-}$ (Figure 3.3a). Cyclic voltammograms recorded at pH 7.0 revealed that the second reduction of the cobalt porphyrin complexes, which leads either to Co(I)-porphyrins (Co^{I}-P) or to Co(II)-porphyrin radical anion (Co^{II}-$P^{\bullet-}$) species, induces electrocatalytic hydrogen evolution, with an onset potential (with catalytic current higher than −20 µA) at −0.84 to −1.04 V vs. NHE depending on the substituents (Figure 3.3b). Since the redox potential of the $[Ru(bpy)_3]^{2+}/[Ru(bpy)_3]^{+}$ couple is reported to lie between −1.26 and −1.32 V vs. NHE,[13,44,45] the one-electron reduced species PS^{-}, corresponding to $[Ru(bpy)_3]^{+}$, is capable to thermodynamically drive the reduction of all four Co(III)-porphyrins

to a potential where the catalytic HER occurs, with an electron-transfer driving force E_{dr} (Figure 3.1) being larger than 160 mV. It is worth noting that for $[Co\text{-}F16P]^{3-}$ a small reduction wave is present at −0.80 V vs. NHE at the foot of the catalytic wave (Figure 3.3b). Interestingly, a similar reduction wave was observed for the $[Zn\text{-}F16P]^{4-}$ analogue, for which metal-based reduction is nearly impossible (Figure 3.3c). This reduction must hence be ligand-based.

LSV of the Zn-porphyrin complexes were measured at pH 7.0 to focus on their electrochemical reduction processes. As expected, the more electron-poor $[Zn\text{-}F16P]^{4-}$ showed the least negative reduction potential (−0.80 V vs. NHE, see Figure 3.3c). The reduction current did not increase significantly with more negative potential until −1.10 V vs. NHE, which suggested this reduction was a reduction process of the complex without catalysis. In addition, the reduction current was around −8 µA which was similar to the current of 1-e^- reduction of Co^{III} to Co^{II} −7 µA (Figure AII.7). Thus, this first reduction process was considered to be 1-electron; it was also observed for $[Zn\text{-}F8P]^{4-}$ but not for the more electron-rich zinc porphyrin complexes $[Zn\text{-}MeP]^{4-}$ and $[Zn\text{-}OMeP]^{4-}$. Significant reduction of $[Zn\text{-}MeP]^{4-}$ and $[Zn\text{-}OMeP]^{4-}$ was observed below −1.20 V vs. NHE with reduction current higher than −16 µA; these two compounds hence underwent a reduction process with more than $2e^-$ (Figure AII.8). We tentatively ascribe this process to the electrocatalytic HER, which takes place at the same potential as the reduction of $[Zn\text{-}F8P]^{4-}$ and $[Zn\text{-}F16P]^{4-}$. Overall, in aqueous solution at pH 7.0 the reduced form of the photosensitizer, $[Ru(bpy)_3]^+$, should also be capable to drive the 2-electron reduction of the Zn-porphyrin complexes and the HER, with a driving force E_{dr} that is higher than 60 mV.

CVs recorded at pH 4.1, show that all Co-porphyrin complexes are also electrocatalytically active for the HER at this pH (Figure 3.3d). As expected, the compounds $[Co\text{-}OMeP]^{3-}$, $[Co\text{-}MeP]^{3-}$ and $[Co\text{-}F8P]^{3-}$ show a higher catalytic current at pH 4.1 than at pH 7.0. However, the electrocatalytic current obtained with $[Co\text{-}F16P]^{3-}$ was lower at pH 4.1 (< −100 µA) than at pH 7.0 (> −200 µA), with 200 mV more over potential. This unexpected result strongly suggests that this electron-poor catalyst may catalyze the HER at neutral pH more efficiently than at pH 4.1, possibly by following a different mechanism than the other complexes.

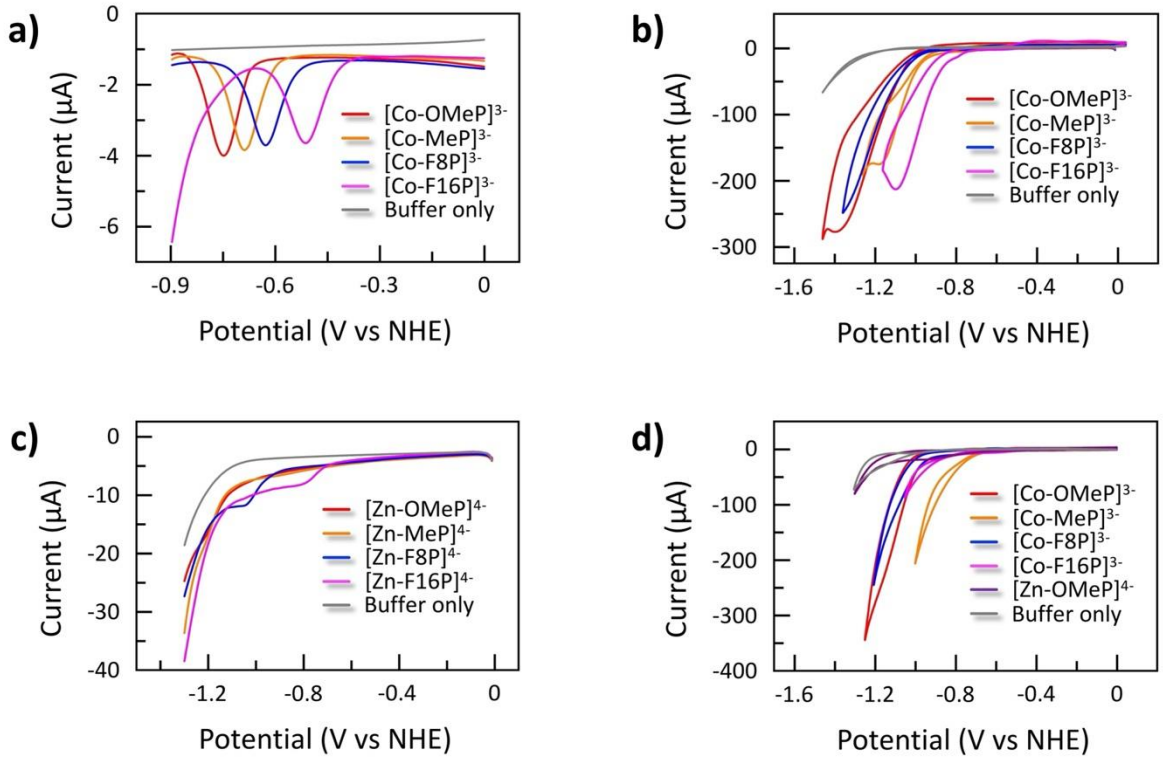

Figure 3.3 *Electrochemistry at pH 7.0 and 4.1 of the water-soluble metal porphyrin complexes studied in this work. a) Differential pulse voltammetry (DPV) and b) cyclic voltammetry (CV) of the Co(III) complexes at pH 7.0; c) linear sweep voltammetry (LSV) of the Zn(II) porphyrin complexes at pH = 7.0 and d) CV of the Co-porphyrin complexes at pH = 4.1. Conditions: 0.1 M phosphate buffer, 0.07 cm^2 glassy-carbon working electrode, Pt wire auxiliary electrode, Ag/AgCl reference electrode, CV and LSV scan rate 50 mV s^{-1}, T = 298 K. DPV experimental parameters: 0.004 V increase potential, 0.05 V amplitude, 0.05 s pulse width, 0.0167 s sampling width, 0.5 s sample period.*

3.2.3 Photocatalysis

Considering the encouraging electrocatalytic results described above, the photocatalytic activity of all metal porphyrin complexes in HER was tested in homogeneous aqueous solutions using $[Ru(bpy)_3]Cl_2$ as PS (0.5 mM), AA and TCEP (100 mM each) as the sacrificial electron donors, under blue light (450 nm, 16 mW) irradiation. Unlike under electrocatalytic conditions, where all Co-porphyrins showed catalytic activity for proton reduction, in photocatalytic conditions at pH = 7.0 only the most electron-poor and the most electron-rich complexes showed significant activity. The electron-poorest Co-porphyrin complex, $[Co\text{-}F16P]^{3-}$, showed the highest turnover number (TON, see Section 3.4.5) after 39.5 h irradiation, of 70 ± 3 mol_{H2}/mol_{HEC} and a maximum turnover frequency (TOF, see Section 3.4.5), of 6.7 ± 0.3 h^{-1}.

By contrast, the most electron-rich complex [Co-OMeP]$^{3-}$ had a lower activity than [Co-F16P]$^{3-}$, while the electron-poor [Co-F8P]$^{3-}$ complex only showed negligible activity and the electron-rich [Co-MeP]$^{3-}$ was not active at all (Figure 3.4a). At that stage it was surprising to find [Co-F16P]$^{3-}$ so active at pH 7.0, as for this complex the driving force for electron transfer E_{dr} (Figure 3.1) was 110 mV stronger than that found for [Co-MeP]$^{3-}$ according to their onset potential of –0.84 and –0.95 V vs. NHE (Table 3.1), while [Co-MeP]$^{3-}$ showed no photocatalytic activity in such conditions.

Table 3.1 *Electrochemical properties of Co-porphyrin complexes at pH 7.0 and pH 4.1.*

	1st reduction potential at pH 7.0 (at pH 4.1)[a]	**HER on-set potential at pH 7.0 (at pH 4.1)[b]**	**η at pH 7.0 (at pH 4.1)[c]**	**E_{dr} at pH 7.0 (at pH 4.1)[d]**
[Co-OMeP]$^{3-}$	−0.75 (−0.78)	−1.04 (−0.95)	630 (710)	220 (310)
[Co-MeP]$^{3-}$	−0.70 (−0.73)	−0.95 (−0.74)	540 (500)	310 (520)
[Co-F8P]$^{3-}$	−0.64 (−0.66)	−1.01 (−0.94)	600 (700)	250 (320)
[Co-F16P]$^{3-}$	−0.53 (−0.55)	−0.84 (−0.88)	430 (640)	420 (380)

[a] data according to DPV, V vs. NHE. [b] data according to CV, V vs. NHE. [c] calculated according to the HER on-set potential, in mV. [d] calculated according to $E_{PS}(PS/PS^{-}) = -1.26$ V vs. NHE, in mV.

At pH 4.1, the photocatalytic HER activity of electron-rich compounds [Co-OMeP]$^{3-}$ and [Co-MeP]$^{3-}$ as well as the electron-poor compound [Co-F8P]$^{3-}$, all improved compared with pH 7. After 39.5 h irradiation, [Co-OMeP]$^{3-}$ showed the highest TON of 175 ± 5 mol_{H2}/mol_{HEC} with a maximum TOF of 7.2 ± 0.4 TON/h, while [Co-MeP]$^{3-}$, which was not active at pH 7.0, at pH 4.1 showed a TON of 22. [Co-F8P]$^{3-}$ showed a very fast turnover at the beginning of the reaction (12.7 h^{-1}), but the system was not stable resulting after 39.5 h in a TON of only 80. Surprisingly, however, the electron-poorest complex [Co-F16P]$^{3-}$ showed a significantly lower photocatalytic activity at pH 4.1 (Figure 3.4b), characterized by a TON of 10 after 39.5 h irradiation, while at pH 7.0 in otherwise identical conditions a TON of 70 was reached.

All together, these photocatalytic results are consistent with those observed in electrochemical conditions. The electron-withdrawing fluorine substituents not only seem to influence the electron density of the metal center, but also to change the pH dependence of the catalytic activity, which are reversed to that of electron-rich cobalt catalysts. This, in turn, suggests that the mechanism of catalytic proton reduction at the porphyrin complexes are different for the electron-rich and electron-poor cobalt compounds.

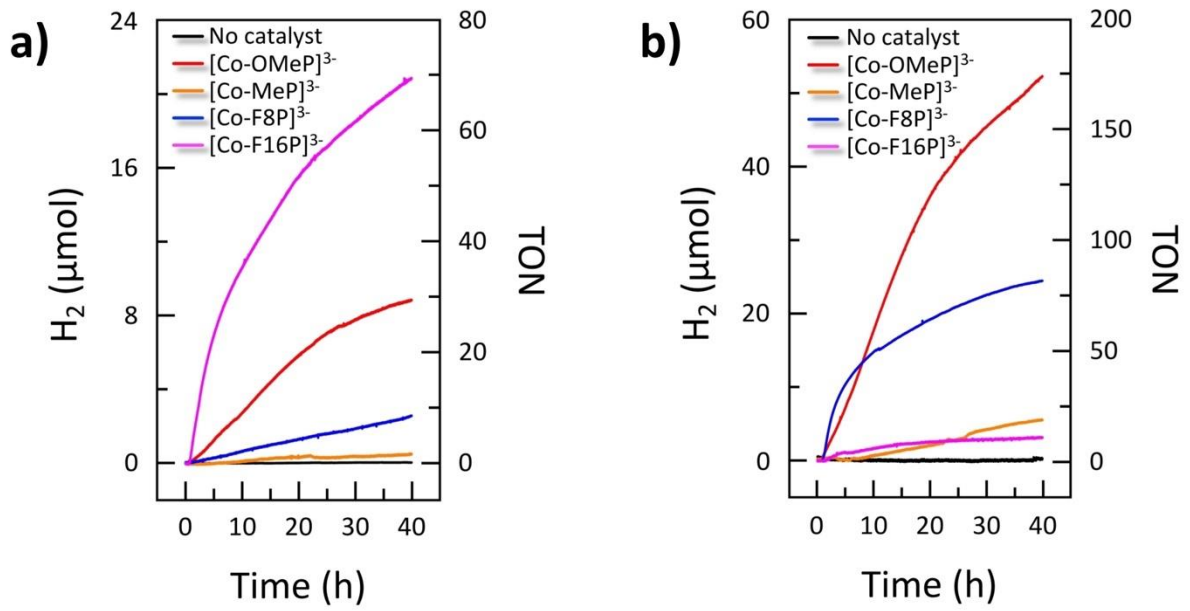

Figure 3.4 *Hydrogen evolution during photocatalytic water reduction in homogeneous aqueous solution in presence of 0.1 mM catalyst [Co-OMeP]$^{3-}$, [Co-MeP]$^{3-}$, [Co-F8P]$^{3-}$ or [Co-F16P]$^{3-}$, 0.5 mM [Ru(bpy)$_3$]Cl$_2$ as photosensitizer, 0.1 M ascorbate and TCEP as electron donor, at pH 7.0 (a) or 4.1 (b), using blue light irradiation (450 nm, 16 mW). Conditions: T = 298 K, phosphate aqueous buffer.*

Photocatalytic hydrogen evolution using the Zn-porphyrin complexes as catalysts was also investigated using the same conditions as described above. In the zinc complexes, only the ligand may lead to HEC activity, as the metal center is unable to accommodate different redox states. At pH 7.0 only use of the electron-poor Zn-porphyrin complexes resulted in significant HER activity. [Zn-F16P]$^{4-}$ reached a TON of 9.5 after 39.5 h irradiation (Figure AII.9), while [Zn-F8P]$^{4-}$ showed lower activity (TON = 6.5). This observation confirmed not only that a ligand-based catalytic pathway for HER is possible with these porphyrins, but also that catalysis becomes faster when more electron-withdrawing groups are added to the porphyrin ring. As a note, in these neutral conditions [Zn-F16P]$^{4-}$ and its free-base analogue [H$_2$-F16P]$^{4-}$ (which is also active for photocatalytic HER) showed lower photocatalytic activity than [Co-F16P]$^{3-}$ (Figure AII.10a). Therefore, the mechanism of HER with [Co-F16P]$^{3-}$ as catalyst must not only involve the ligand, but also the cobalt center in the different intermediates. In contrast, at pH 4.1 [Zn-OMeP]$^{4-}$ was found to be inactive (Figure AII.10b), while [Co-OMeP]$^{3-}$ showed the highest photocatalytic activity. This result suggests that for the most electron-rich cobalt catalyst of this series the high activity in acidic conditions involves mainly the metal center.

The influence of pH on the photocatalytic activity of $[Co\text{-}OMeP]^{3-}$ and $[Co\text{-}F16P]^{3-}$ was further studied at different pH values between 4.1 and 9.0, using otherwise identical conditions. Upon increasing the pH from 4.1 to 7.0, the TON after 39.5 h for $[Co\text{-}F16P]^{3-}$ increased from 10 to 70, but the TON decreased to 12 upon further increase of the pH to 9.0 (Figure 3.5a and AII.11a). Thus, for this complex pH 7.0 appears to be optimal for the stability of the photocatalytic system, although a higher maximum TOF of 8.9 TON/h was found at pH 6.0 (Figure AII.11b). By contrast, the electron-rich complex $[Co\text{-}OMeP]^{3-}$ clearly showed increasing TON and TOF with more acidic pH, culminating in a TON of 175 and a TOF of 7.2 TON/h at pH 4.1 (Figure 3.5b and AII.11).

Thus, classical behavior is observed for the electron-rich complex $[Co\text{-}OMeP]^{3-}$, with faster H_2 generation at low pH values. For the electron-poor complex $[Co\text{-}F16P]^{3-}$, at pH values higher than 7.0 the HER activity becomes (of course) limited by the low proton concentration hampering the formation of a Co(III) hydride species. More striking, however, is the observation that a high proton concentration significantly inhibits catalytic activity as well. The most favorable condition for this catalyst is pH 7.0, in which use of $[Co\text{-}F16P]^{3-}$ results in a two times higher TON than the use of $[Co\text{-}OMeP]^{3-}$.

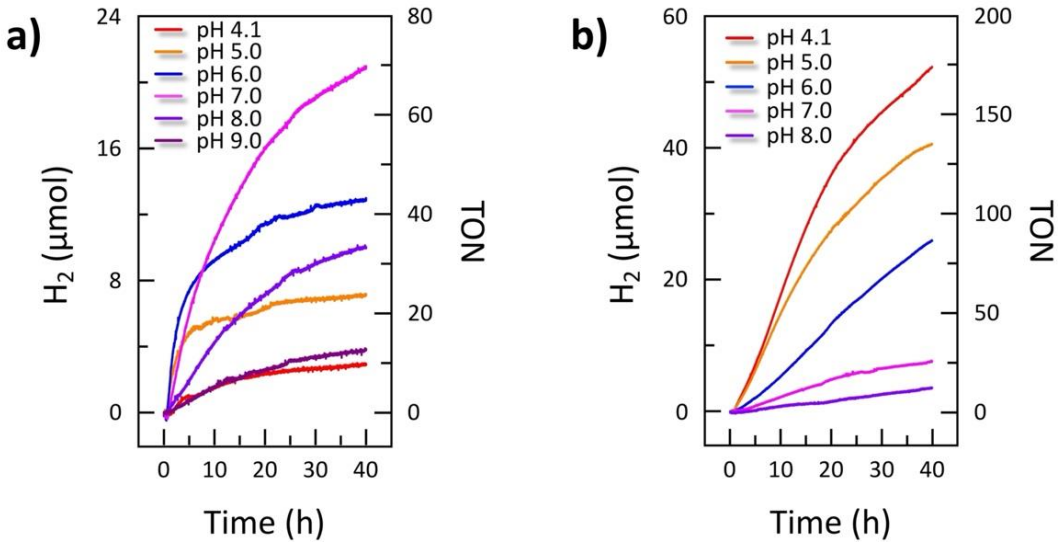

Figure 3.5 *Hydrogen evolution during photocatalytic water reduction in presence of a) 0.1 mM catalyst* $[Co\text{-}F16P]^{3-}$ *and b)* $[Co\text{-}OMeP]^{3-}$ *at different pH in aqueous solution using 0.5 mM* $[Ru(bpy)_3]Cl_2$ *as photosensitizer, 0.1 M ascorbic acid and TCEP as electron donor, and blue light irradiation (450 nm, 16 mW). Conditions: T = 298 K, phosphate buffer.*

In order to check the photostability of $[Co\text{-}F16P]^{3-}$ and $[Co\text{-}OMeP]^{3-}$, the UV-vis spectra of solutions of complexes in 0.1 M phosphate buffer (pH 7.0) were monitored either in the dark

or upon blue light irradiation for 48 h (450 nm, 16 mW). After 48 h irradiation, the UV-vis spectra of $[Co\text{-}F16P]^{3-}$ and $[Co\text{-}OMeP]^{3-}$ had changed only slightly (Figure AII.12 and AII.13), in contrast with $[Zn\text{-}OMeP]^{4-}$, which lost 80% of its absorption properties after 48 h of irradiation at 423 nm. In another experiment using $[Co\text{-}F16P]^{3-}$ or $[Co\text{-}OMeP]^{3-}$ as the catalyst, two consecutive photocatalytic runs were performed, adding a fresh batch of PS between the two runs to compensate for possible PS decomposition. Only 3-5% lower TON were found after the second photocatalytic run (Figure AII.14). As widely reported, $[Ru(bpy)_3]^{2+}$ decomposes quickly in photocatalytic aqueous conditions,[13,46] which is responsible for the deactivation of the HER photocatalytic system. Overall, these results confirm the excellent photostability of both $[Co\text{-}F16P]^{3-}$ and $[Co\text{-}OMeP]^{3-}$.

3.2.4 Kinetic study

A full kinetic study was performed of the photocatalytic system at pH 7.0 using the catalyst $[Co\text{-}F16P]^{3-}$. The light intensity and the concentration of the electron donors, the PS, and the catalyst, were systematically varied. It appeared that the maximum rate of hydrogen evolution of the system did not change significantly when the light power was higher than 10 mW (Figure 3.6a), when the concentration of ascorbate and TCEP was higher than 0.075 M (Figure 3.6b), or with a PS concentration higher than 0.25 mM (Figure 3.6c). However, a first-order dependence of the maximum H_2 evolution rate was found on catalyst concentration (Figure 3.6d). The observation that the photon flux, the concentration of sacrificial electron donor, and the photosensitizer concentration, do not influence, in our standard photocatalytic conditions (0.1 mM catalyst, 0.5 mM $[Ru(bpy)_3]Cl_2$, 0.1 M ascorbate and TCEP, 450 nm, 16 mW), the maximum rate of hydrogen evolution of this system means that Step 1, Step 2 and Step 3 in Figure 3.1 are not limiting the photocatalytic reaction rate. The rate-determining step (RDS) of the system appears to be Step 4, i.e., the catalytic H_2-evolving step. Considering the linear dependence of the H_2 production rate with catalyst concentration, it appears that the rate-determining step of the catalytic cycle involves one molecule of $[Co\text{-}F16P]^{3-}$. Using 0.1 mM $[Co\text{-}F16P]^{3-}$ in the standard conditions at pH 7.0, the quantum yield for H_2 evolution was calculated to be 0.10 ± 0.01%. This low quantum yield highlights the occurrence of many charge-recombination events that are characteristic of homogeneous photocatalytic systems.

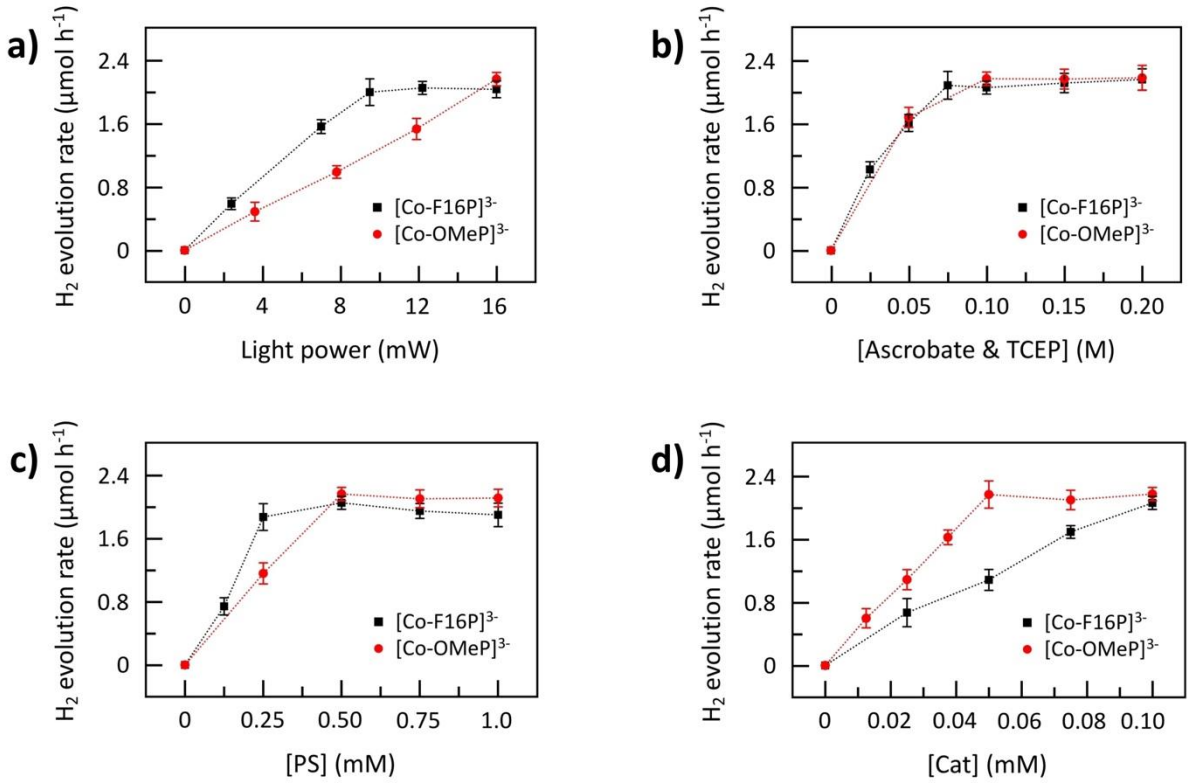

Figure 3.6 *Maximum H_2 evolution rate during photocatalytic H_2 evolution using the catalyst [Co-F16P]$^{3-}$ at pH 7.0 (black squares) or [Co-OMeP]$^{3-}$ at pH 4.1 (red circles) plotted as a function of a) the light power, b) the concentration of ascorbate and TCEP, c) the concentration of the photosensitizer $[Ru(bpy)_3]Cl_2$ and d) the concentration of the catalyst. Standard conditions: 0.1 mM catalyst, 0.5 mM $[Ru(bpy)_3]Cl_2$, 0.1 M ascorbate and TCEP, blue light (450 nm, 16 mW), T = 298 K.*

A similar kinetic study was performed at pH 4.1 using the catalyst [Co-OMeP]$^{3-}$, for which significantly different results were obtained. A first-order dependence of the maximum H_2 evolution rate on light power was found (Figure 3.6a), indicating that the RDS of this catalytic system involves the photon flux, and thus is related to Step 1 in the mechanism. Clearly, for this electron-rich catalyst and at that low pH, Step 4 is relatively fast, at least as soon as the catalyst concentration is high enough ([Cat] > 0.05 mM). In addition, a first-order dependence of the maximum hydrogen evolution rate on the catalyst concentration was found at low concentrations of [Co-OMeP]$^{3-}$, i.e. 0.05 mM or lower (Figure 3.6d), suggesting that the catalytic H_2 evolution involves one molecule of catalyst, but that at higher HEC concentrations the photon flux becomes limiting, which is similar as the result reported by Alberto and coworkers.[47] Using 0.1 mM [Co-OMeP]$^{3-}$ in the standard conditions at pH 4.1, the quantum yield for H_2 evolution was calculated to be 0.12 ± 0.01%, which is very similar to that for [Co-

F16P]$^{3-}$ at pH 7.0. Clearly, while their mechanisms seem to be different, the performances of both catalysts in optimized conditions were actually comparable.

3.2.5 Discussion

On the one hand, the electrochemical properties of the Co-porphyrin complexes show that the electron-richness of the ligand controls the first reduction potential of the complex, i.e, from Co^{III}-P to Co^{II}-P, which does not lead to hydrogen evolution (note that hereafter and in Figure 3.8, the notation P represents the hexaanionic porphyrin ligand). The second reduction, on the other hand, does lead to catalytic hydrogen evolution, but its dependence on the electronic properties of the substituents is less straightforward to establish. The electron-richest complex [Co-OMeP]$^{3-}$ has the most negative onset potentials of –1.04 and –0.95 V vs. NHE at pH 7.0 and pH 4.1, respectively (Table 3.1). However, the electron-poorest complex [Co-F16P]$^{3-}$ has the least negative onset potential of –0.84 V vs. NHE only at pH 7.0. At pH 4.1 it is [Co-MeP]$^{3-}$ that has the least negative onset potential of –0.74 V vs. NHE. Therefore, the E_{dr} value of these Co-porphyrin systems, calculated by the difference between $E_{PS}(PS/PS^{-})$ and the hydrogen evolution onset potential of the catalyst, does not simply depend on the electron-richness of the catalyst. This observation is valid at both pH 7.0 and pH 4.1. The lower value of E_{dr} for [Co-F16P]$^{3-}$ when the pH goes from 7.0 (420 mV) to 4.1 (380 mV) suggests that a faster electron transfer from the photo-reduced species PS^{-} to [Co-F16P]$^{3-}$ may occur at pH 7.0 than at pH 4.1. Indeed, the kinetic study in photocatalytic conditions demonstrated that when using standard concentrations (0.1 mM catalyst, 0.5 mM $[Ru(bpy)_3]Cl_2$, 0.1 M ascorbate and TCEP) and light intensities (450 nm, 16 mW), the rate of the photocatalytic system using [Co-F16P]$^{3-}$ as HEC at pH 7.0 was limited by the catalytic HER. As a consequence, the electron transfer between PS^{-} and HEC does not limit the HER rate, and the E_{dr} value of this system is "high enough". At pH 4.1 and using identical concentrations and light intensity, the catalytic step of the photocatalytic system using [Co-OMeP]$^{3-}$ as HEC was limited by the photon flux; in other terms, this HEC was "fast enough", and E_{dr} was also high enough. Overall, both at pH 7.0 and 4.1 the onset potential of the catalyst in electrocatalytic conditions did not allow to predict the activity in photocatalytic conditions. In fact, the difference in performance between the photocatalytic systems using [Co-OMeP]$^{3-}$ at pH 4.1 and that using [Co-F16P]$^{3-}$ at pH 7.0 appears to be mainly due to the differences in their HER catalytic mechanisms.

For the electron-rich HEC [Co-OMeP]$^{3-}$, the better catalytic properties at lower pH and the absence of catalytic activity of the zinc analogue suggest that catalytic hydrogen generation

occurs via a metal-based pathway.[4] This behavior is typical for many metal-based catalysts,[9] and the generally accepted mechanism is shown in Figure 3.8. Co^{III}-P is first reduced by PS^{-} to Co^{II}-P, after which a second reduction by PS^{-} results in formation of Co^{I}-P. Protonation of this species then forms the cobalt(III)-hydride intermediate H-Co^{III}-P. Alternatively, protonation of Co^{II}-P to H-Co^{IV}-P may occur first, which is followed by a second reduction to form the same intermediate H-Co^{III}-P. Reaction with a second proton releases H_2 via a heterolytic route known as protonolysis, regenerating Co^{III}-P.[9] The ability of the metal center to accommodate several oxidation states is critical for this mechanism to take place.

On the other hand, porphyrin ligands can be redox non-innocent,[1,48,49] in particular when they are modified with strong (or many) electron-withdrawing substituents, which makes the porphyrin ring more likely to be reduced to a radical anion. Next to the metal-based pathway alternative catalytic pathways have been suggested for the HER catalyzed by Co-porphyrins, based on reduction of either the ligand alone, or on a combination of the metal and the ligand. Here we hypothesize that ligand reduction may be the reason for $[Co\text{-}F16P]^{3-}$ having an additional reduction wave at the foot of its catalytic current at −0.80 V vs. NHE at pH 7.0 (Figure 3.3b), which is tentatively attributed to formation of a Co(II)-($P^{\bullet-}$) radical ligand species. This reduction wave is also present in the LSV of the $[Zn\text{-}F16P]^{4-}$ compound at a similar potential (Figure 3.3c), as both complexes share the same ligand. In addition, the zinc analogue $[Zn\text{-}F16P]^{4-}$ is also photocatalytically active, albeit to a lesser extent. In photocatalytic conditions, such redox non-innocence of the ligand leads to a very different pH dependence of the H_2-evolution properties of the complex. We hence propose $[Co\text{-}F16P]^{3-}$ to catalyze hydrogen evolution via a mixed metal- and ligand-based mechanism. In such a mechanism (Figure 3.8), the H-Co^{IV}-P species can be reduced to a H-Co^{IV}-($P^{\bullet-}$) species via a one-electron reduction of the porphyrin ring.[1] Here a ligand-to-metal charge transfer (CT) may take place to transfer the H-Co^{IV}-($P^{\bullet-}$) species to H-Co^{III}-P and then release H_2 after reacting with a second electron; or directly be protonated again forming a Co^{IV}-H-H-($P^{\bullet+}$) species that evolves H_2 by the so-called "homolytic" route (Figure 3.8). Since the 1 e^--reduction of Co^{II}-P may also take place at the porphyrin ring, Co^{II}-($P^{\bullet-}$) may be formed first, which is protonated to form a ligand-based hydride species Co^{II}-($P^{\bullet+}$)-H that could either react on the metal with a proton to form a Co^{IV}-H-H-($P^{\bullet+}$) species, or undergo a metal-to-ligand CT forming a Co^{III}-P-H species to finally give H_2 and Co^{III}-P. This kind of metal-to-ligand CT may also occur when Co^{II}-P undergoes protonation forming a Co^{III}-P($^{\bullet+}$)-H analogue intermediate, which could be further reduced by 1 e^- to Co^{II}-($P^{\bullet+}$)-H or Co^{III}-P-H. The Co^{III}-P-H species finally could release H_2 by protonation

via a "heterolytic", ligand-based pathway. Since neutral pH was optimum for the photocatalytic HER using [Co-F16P]$^{3-}$, the key Co^{IV}-H-H-($P^{\bullet+}$) species is proposed to be generated more likely in neutral conditions. A high proton concentration may cause decoordination of the cobalt center from the porphyrin ligand, leading to the deactivation of the catalytic system. Alternatively, a high concentration of proton may prevent the formation of some key intermediates for hydrogen generation; this hypothesis is currently investigated in a collaboration to perform a DFT modeling study.

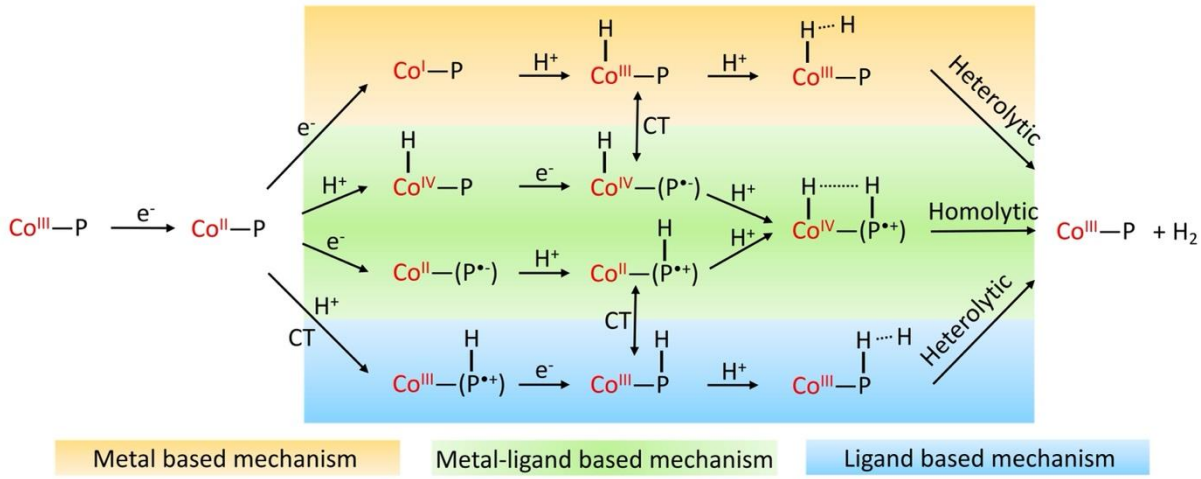

Figure 3.8 *Proposed hydrogen evolution mechanisms with Co-porphyrin complex as catalyst. P represents a hexaanionic porphyrin ligand. CT = charge transfer.*

3.3 Conclusion

A series of tetra-anionic Co- and Zn-porphyrin complexes were prepared and tested as catalysts for homogeneous photocatalytic hydrogen evolution from water in neutral and acid conditions. Their catalytic activity and catalytic mechanism were strongly dependent on the presence of electron-withdrawing or electron-donating substituents on the porphyrin. For the electron-richest catalyst [Co-OMeP]$^{3-}$, which has on paper a stronger driving force to reduce water, higher photocatalytic activities were observed as expected, but only at low pH (4.1). In neutral conditions, its activity was much lower, and completely vanished when the cobalt center was replaced by zinc. By contrast, for the electron-poorest catalyst [Co-F16P]$^{3-}$, photocatalytic hydrogen evolution was comparatively low at pH 4.1, but it was much better than [Co-OMeP]$^{3-}$ at neutral pH, resulting in comparable photocatalytic H_2 production quantum yields, compared to that obtained with [Co-OMeP]$^{3-}$ at pH 4.1. For [Co-F16P]$^{3-}$, the second catalyst reduction step by PS^- probably occurred via a pathway involving both the metal and the ligand, and when

replacing cobalt for zinc, part of the ligand-based photocatalytic activity was retained. This work represents a significant advance in the understanding of how molecular hydrogen evolution catalyst should be designed, because it indicated that it is not necessary to functionalize HER catalysts with electron-donating groups to enhance their catalytic activity, in particular in pH-neutral conditions. Electron-withdrawing groups lead to good catalysts at pH 7.0, too, but with a mechanism that differs from that obtained with electron-rich complexes at lower pH. In systems coupling photocatalytic HEC and OEC near pH 7.0, electron-poor proton reduction catalysts may represent a better optimum than the usually proposed electron-rich catalysts.

3.4 Experimental section

3.4.1 Materials and methods

All reagents were purchased from Sigma-Aldrich and used as received unless otherwise noted. The compounds tetrasodium-5,10,15,20-tetrakis(2,6-dimethoxyphenyl-3-sulfonatophenyl)-21*H*,23*H*-porphyrin ($Na_4[H_2$-OMeP]),[8] tetrasodium-5,10,15,20-tetrakis(2,6-dimethylphenyl-3-sulfonatophenyl)-21*H*,23*H*-porphyrin ($Na_4[H_2$-MeP]),[37] tetrasodium-2,3,7,8,12,13,17,18-octafluoro-5,10,15-20-tetrakis(2,6-difluoro-3-sulfonatophenyl)-21*H*,23*H*-porphyrin ($Na_4[H_2$-F16P]),[39] trisodium-5,10,15,20-tetrakis(2,6-difluoro-3-sulfonatophenyl)porphyrin-Co(III) (Na_3[Co-F8P]),[40,41] tetrasodium-5,10,15,20-tetrakis(2,6-difluoro-3-sulfonatophenyl)porphyrin-Zn(II) (Na_4[Zn-F8P]),[42] tetrasodium-2,3,7,8,12,13,17,18-octafluoro-5,10,15-20-tetrakis(2,6-difluoro-3-sulfonatophenyl)porphyrin-Zn(II) (Na_4[Zn-F16P]),[39] were prepared according to published methods. ^{1}H NMR spectra were recorded on a Bruker 400DPX-liq spectrometer operating at 400 MHz. ^{19}F NMR spectra were recorded on a Bruker 500DPX spectrometer operating at 500 MHz. High-resolution mass spectrometric measurements were made on a Bruker Fourier Transform Ion Cyclotron Resonance Mass Spectrometer APEX IV at Leiden University. Elemental analyses were performed at the Mikroanalytisches Laboratorium Kolbe, Germany. Electronic absorption spectra were obtained on a Varian Cary 60 spectrophotometer at 25 °C during the spectrophotometric measurements. The LED optical power was measured using an OPHIR Nova-display laser power meter.

3.4.2 Synthesis

Trisodium 5,10,15,20-tetrakis(2,6-dimethoxyl-3-sulfonatophenyl)porphyrin cobalt(III) (Na_3[Co-OMeP])

The ligand $Na_4[H_2$-OMeP] (115 mg, 0.09 mmol) and Milli-Q water (40 mL) were placed under N_2 in a 100 mL round-bottom flask equipped with a magnetic stirring bar and a condenser. A solution of cobalt(II) sulfate heptahydrate (126 mg, 0.45 mmol) in Milli-Q water (10 mL) was added to the stirred solution, and the mixture was refluxed for 12 h under N_2. After cooling to room temperature, water was rotary evaporated at 40 °C and the residue was redissolved in cold methanol (15 mL). After filtration on a filter paper, methanol was rotary-evaporated, the residue was redissolved in cold methanol (5 mL). The solution was filtered by filter paper, rotary-evaporated, and the crude product was redissolved in Milli-Q water (5 mL) then passed onto an Amberlite IR 120 Na^+ form ion exchange resin column (10 cm), washed with Milli-Q water and further purified on Sephadex-20H size exclusion chromatography to remove excess cobalt sulfate (methanol). Methanol was finally rotary evaporated and the solid dried in vacuo. Yield (115 mg, 88%); ^{1}H NMR (400 MHz, CD_3OD): δ = 9.37 – 9.19 (m, 8H; β-pyrrole-H), 8.48 – 8.40 (m, 4H; *p*-Ph-H), 7.52 – 7.15 (m, 4H; *m*-Ph-H), 3.92 – 3.49 (m, 12 H; OCH_3), 3.24 – 2.29 ppm (m, 12 H; OCH_3); HRMS (ESI): *m*/*z* calcd for $C_{52}H_{44}N_4CoO_{20}S_4^+$: 1231.0758 [*M*-3Na+4H]$^+$; found: 1231.0750; elemental analysis calcd (%) for $C_{52}H_{40}N_4Na_3CoO_{20}S_4 \bullet Na_2SO_4 \bullet H_2O$: C 42.86, H 2.91, N 3.85; found: C 43.01, H 2.79, N 3.84. UV-vis (H_2O): λ_{max}(ε in M^{-1} cm^{-1}) 426 nm (8.8×10^4), 542 nm (5.8×10^3).

Trisodium 5,10,15,20-tetrakis(2,6-dimethyl-3-sulfonatophenyl)porphyrin cobalt(III) (Na_3[Co-MeP])

Tetrasodium 5,10,15,20-tetrakis(2,6-dimethyl-3-sulfonatophenyl)-21*H*,23*H*-porphyrin·$9H_2O$ (130 mg, 0.10 mmol) and Milli-Q water (40 mL) were placed under N_2 in a 100 mL round-bottom flask equipped with a magnetic stirring bar and a condenser. A solution of cobalt(II) sulfate heptahydrate (141 mg, 0.50 mmol) in Milli-Q water (10 mL) was added to the stirred solution and the mixture was refluxed for 12 h under N_2. After cooling to room temperature, water was rotary evaporated and the residue was redissolved in cold methanol (15 mL). After filtration on a filter paper, methanol was rotary-evaporated, the residue was redissolved in cold methanol (5 mL), the solution was filtered a second time by filter paper and rotary-evaporated, then the crude product was then passed onto an Amberlite IR 120 Na^+ form ion exchange resin column (10 cm), washed with Milli-Q water and finally purified on Sephadex-20H size exclusion chromatography (methanol). Methanol was finally rotary

evaporated and the solid dried in vacuo. Yield (109 mg, 90%); ^{1}H NMR (400 MHz, CD_3OD): δ = 9.18 – 9.09 (m, 8H; β-pyrrole-H), 8.43 – 8.38 (m, 4H; *p*-Ph-H), 7.68 – 7.55 (m, 4H; *m*-Ph-H), 2.42 – 2.09 (m, 12H; CH_3), 2.07 – 1.74 ppm (m, 12H; CH_3); HRMS (ESI): *m*/*z* calcd for $C_{52}H_{43}N_4NaCoO12S4^+$: 1125.0985 [*M*-2Na+3H]$^+$; found: 1125.0977; elemental analysis calcd (%) for $C_{52}H_{40}N_4Na_3CoO_{12}S_4$•$2H_2O$: C 51.83, H 3.68, N 4.65; found: C 52.08, H 3.43, N 4.66. UV-vis (H_2O): λ_{max}(ε in M^{-1} cm^{-1}) 428 nm (2.3×10^5), 545 nm (1.2×10^4).

Trisodium 2,3,7,8,12,13,17,18-octafluoro-5,10,15-20-tetrakis(2,6-difluoro-3-sulfonatophenyl)porphyrin cobalt(III) (Na_3[Co-F16P])

Tetrasodium 2,3,7,8,12,13,17,18-octafluoro-5,10,15,20-tetrakis(2,6-difluoro-3-sulfonatophenyl)-21*H*,23*H*-porphyrin•$5H_2O$ (140 mg, 0.10 mmol) and Milli-Q water (40 mL) were placed under N_2 in a 100 mL round-bottom flask equipped with a magnetic stirring bar and a condenser. A solution of cobalt(II) sulfate heptahydrate (141 mg, 0.50 mmol) in Milli-Q water (10 mL) was added to the stirred solution and the mixture was refluxed for 12 h under N_2. After cooling to room temperature, the water was rotary evaporated and the residue was redissolved in cold methanol (15 mL). After filtration over a filter paper, methanol was rotary-evaporated, the residue was redissolved in cold methanol (5 mL), and filtered by filter paper again. The filtrate was rotary-evaporated and the Co-F16 complex was then passed through an Amberlite IR 120 Na^+ form ion exchange resin column (10 cm) and washed with Milli-Q water before being purified on Sephadex-20H size exclusion chromatography (eluent: methanol). Methanol was finally rotary evaporated and the solid dried in vacuo. Yield (135 mg, 90%); ^{1}H NMR (400 MHz, CD_3OD): δ = 6.80 (s, 4H; *p*-Ph-H), 5.60 – 5.37 ppm (m, 4H; *m*-Ph-H); ^{19}F NMR (471 MHz, CD_3OD): δ = -111.97 (d, *J* = 236.0 Hz, 8F; β-pyrrole-F), -112.74 (s, 4F; *o*-F), -113.26 ppm (s, 4F; *o*-F); HRMS (ESI): *m*/*z* calcd for $C_{44}H_{12}F_{16}N_4CoO_{12}S_4^+$: 1278.8406 [*M*-3Na+4H]$^+$; found: 1278.8407; elemental analysis calcd (%) for $C_{44}H_8F_{16}N_4Na_3CoO_{12}S_4$•$Na_2SO_4$•$H_2O$: C 35.12, H 0.67, N 3.72; found: C 35.06, H 0.61, N 3.82. UV-vis (H_2O): λ_{max}(ε in M^{-1} cm^{-1}) 402 nm (1.4×10^5), 535 nm (6.3×10^3)

Tetrasodium 5,10,15,20-tetrakis(2,6-dimethoxyl-3-sulfonatophenyl)porphyrin zincate(II) (Na_4[Zn-OMeP])

The ligand L-OMe (115 mg, 0.09 mmol) and Milli-Q water (40 mL) were placed under N_2 in a 100 mL round-bottom flask equipped with a magnetic stirring bar and a condenser. A solution of zinc(II) chloride (61 mg, 0.45 mmol) in Milli-Q water (10 mL) was added to the

stirred solution, and the mixture was refluxed for 12 h under N_2. After cooling to room temperature, water was rotary evaporated at 40 °C and the residue was redissolved in cold methanol (15 mL). After filtration on a filter paper, methanol was rotary-evaporated, the residue was redissolved in cold methanol (5 mL). The solution was filtered by filter paper, rotary-evaporated, and the crude product was redissolved in Milli-Q water (5 mL) then passed onto an Amberlite IR 120 Na^+ form ion exchange resin column (10 cm), washed with Milli-Q water and further purified on Sephadex-20H size exclusion chromatography to remove excess zinc chloride (methanol). Methanol was finally rotary evaporated and the solid dried in vacuo. Yield (107 mg, 85%); ^{1}H NMR (400 MHz, CD_3OD): δ = 8.82 – 8.77 (m, 8H; β-pyrrole-H), 8.40 – 8.35 (m, 4H; *p*-Ph-H), 7.31 – 7.23 (m, 4H; *m*-Ph-H), 3.67 – 3.54 (m, 12 H; OCH_3), 3.07 – 2.76 ppm (m, 12 H; OCH_3); HRMS (ESI): *m*/*z* calcd for $C_{52}H_{45}N_4ZnO_{20}S_4^+$: 1237.0796 $[M\text{-}4Na+5H]^+$; found: 1237.0792; elemental analysis calcd (%) for $C_{52}H_{40}N_4Na_4ZnO_{20}S_4 \bullet 4H_2O$: C 44.66, H 3.46, N 4.01; found: C 44.79, H 3.19, N 3.99. UV-vis (H_2O): λ_{max}(ε in M^{-1} cm^{-1}) 422 nm (1.4×10^5), 557 nm (6.5×10^3).

Tetrasodium 5,10,15,20-tetrakis(2,6-dimethyl-3-sulfonatophenyl)porphyrin zincate(II) (Na_4[Zn-MeP])

Tetrasodium 5,10,15,20-tetrakis(2,6-dimethyl-3-sulfonatophenyl)-21*H*,23*H*-porphyrin·$9H_2O$ (130 mg, 0.10 mmol) and Milli-Q water (40 mL) were placed under N_2 in a 100 mL round-bottom flask equipped with a magnetic stirring bar and a condenser. A solution of zinc(II) chloride (68 mg, 0.50 mmol) in Milli-Q water (10 mL) was added to the stirred solution and the mixture was refluxed for 12 h under N_2. After cooling to room temperature, water was rotary evaporated and the residue was redissolved in cold methanol (15 mL). After filtration on a filter paper, methanol was rotary-evaporated, the residue was redissolved in cold methanol (5 mL), the solution was filtered a second time by filter paper and rotary-evaporated, then the crude product was then passed onto an Amberlite IR 120 Na^+ form ion exchange resin column (10 cm), washed with Milli-Q water and finally purified on Sephadex-20H size exclusion chromatography (methanol). Methanol was finally rotary evaporated and the solid dried in vacuo. Yield (110 mg, 90%); ^{1}H NMR (400 MHz, CD_3OD): δ = 8.63 – 8.59 (m, 8H; β-pyrrole-H), 8.35 (m, 4H; *p*-Ph-H), 7.56 – 7.49 (m, 4H; *m*-Ph-H), 2.40 – 2.26 (m, 12H; CH_3), 1.94 – 1.79 ppm (m, 12H; CH_3); HRMS (ESI): *m*/*z* calcd for $C_{52}H_{45}N_4ZnO_{12}S_4^+$: 1109.1203 $[M\text{-}4Na+5H]^+$; found: 1109.1204; elemental analysis calcd (%) for $C_{52}H_{40}N_4Na_4ZnO_{12}S_4 \bullet H_2O$:

C 51.34, H 3.48, N 4.61; found: C 51.54, H 3.39, N 4.61. UV-vis (H_2O): λ_{max}(ε in M^{-1} cm^{-1}) 423 nm (6.0×10^5), 557 nm (1.8×10^4), 599 nm (4.6×10^3).

3.4.3 Cyclic voltammetry, differential pulse voltammetry and linear sweep voltammetry

Cyclic voltammetry (CV), differential pulse voltammetry (DPV) and linear sweep voltammetry (LSV) measurements were performed using an Autolab PGstart10 potentiostat controlled by GPES4 software. All the CV, DPV and LSV measurements were recorded in 0.1 M sodium phosphate buffer (pH 7.0) or 1.0 M sodium phosphate buffer (pH 4.1) using a three-compartment cell possessing a 0.07 cm^2 glassy-carbon electrode as the working electrode, Pt wire as the auxiliary electrode, Ag/AgCl (saturated KCl aq.) as the reference electrode, and $K_3[Fe(CN)_6]$ was added at the end of the measurements as internal standard (E($[Fe(CN)_6]^{3-}$/$[Fe(CN)_6]^{4-}$) = +0.361 V vs NHE).[50] Unless otherwise indicated, the potential was converted relative to NHE, the solutions were bubbled with high-purity argon for at least 30 min before analysis.

3.4.4 Photo-induced hydrogen evolution

Photo-induced hydrogen evolution from water was analysed by a hydrogen electrode (Unisense H2-NP) controlled by x-5 UniAmp using Logger software. The irradiation source was an OSRAM Opto Semiconductors LD W5SM LED (λ_{irr} 450 nm, $\Delta\lambda_{1/2}$ = 25 nm) with water cooling. All the photochemical hydrogen evolution measurements were carried out in a thermostated (298 K) photochemical reactor (total volume 25.0 mL). $[Ru(bpy)_3]Cl_2 \cdot 6H_2O$ (1.3 mg, 0.5 mM), the catalyst Na_3[Co-OMeP], Na_3[Co-MeP], Na_3[Co-F8P], Na_3[Co-F16], Na_4[Zn-OMeP], Na_4[Zn-MeP], Na_4[Zn-F8P], and Na_4[Zn-F16P] (0.1 mM), and ascorbic acid (53 mg, 0.1 M) and tris(2-carboxyethyl)phosphine hydrochloride (86 mg, 0.1 M) were added as solids in the reactor, and dissolved using sodium phosphate buffer (0.1 M, pH 7.0, 3.0 mL), the pH value of the mixture solution was then controlled with sodium hydroxide solid by checking pH. Under constant stirring, the reactor was equipped with 1 rubber septum and 2 silicon septa in order to make an air-tight system (the set-up is shown in Figure AI.29). The hydrogen electrode was then inserted through the septum, to measure the hydrogen concentration in the head space (gas phase) of the photochemical reactor, and the whole system was deaerated by high-purity argon for at least 30 min. After removing the argon, the hydrogen electrode was calibrated by a four-time injection of 100 µL (4.46 µmol at 1 atm) of high-purity H_2 into the closed system, thereby limiting the overpressure to <5%; the calibration was adapted with the pressure change

using Logger software, affording direct reading of the volume of dioxygen (µL) produced in the gas phase of the reactor (V_{gas} = 22.0 mL). Following calibration, the three used septa were replaced by new ones and hydrogen electrode was inserted into the system again. The system was degassed for 30 min with argon, then data recording was started, first keeping the system in the dark for another 30 min prior to starting light irradiation. Unless otherwise indicated, the data recording was stopped after 39.5 h of light irradiation.

3.4.5 Turnover number determination

The turnover number (TON) of oxygen evolution was determined by a hydrogen electrode (Unisense OX-NP) controlled by x-5 UniAmp using Logger software. The amount of oxygen formed during 39.5 h illumination was used to calculate the TON. The TON were calculated from the oxygen production data by the following equation:

$$TON = \frac{n_{O_2}}{n_{cat}}$$

in which n_{O_2} is the number of mol of hydrogen calculated from the volume of the dioxygen produced in the photocatalytic experiment as indicated by the calibrated hydrogen electrode in the gas phase (µL), divided by 22.4 L/mol, and n_{cat} is the number of mol of cobalt and zinc porphyrin catalyst used in the photocatalytic experiment. Errors in triplicate measurements.

The maximum H_2 evolution rate (in h^{-1}) or the maximum turnover frequency TOF_{max} (in h^{-1}) of photocatalytic oxygen evolution was obtained using Origin 9.1 software by 1) nonlinear curve fitting of the time evolution of the TON, starting at t = 30 min for photocatalytic reactions (category: Growth/Sigmoidal, function: logistic Fit); 2) calculating the first derivative TOF = f(t) using mathematics, differentiate, and 3) identify the maximum value of H_2 evolution rate or TOF_{max} of TOF = f(t) (example of $[Co\text{-}OMeP]^{3-}$ see Figure 3.9). Errors in triplicate measurements.

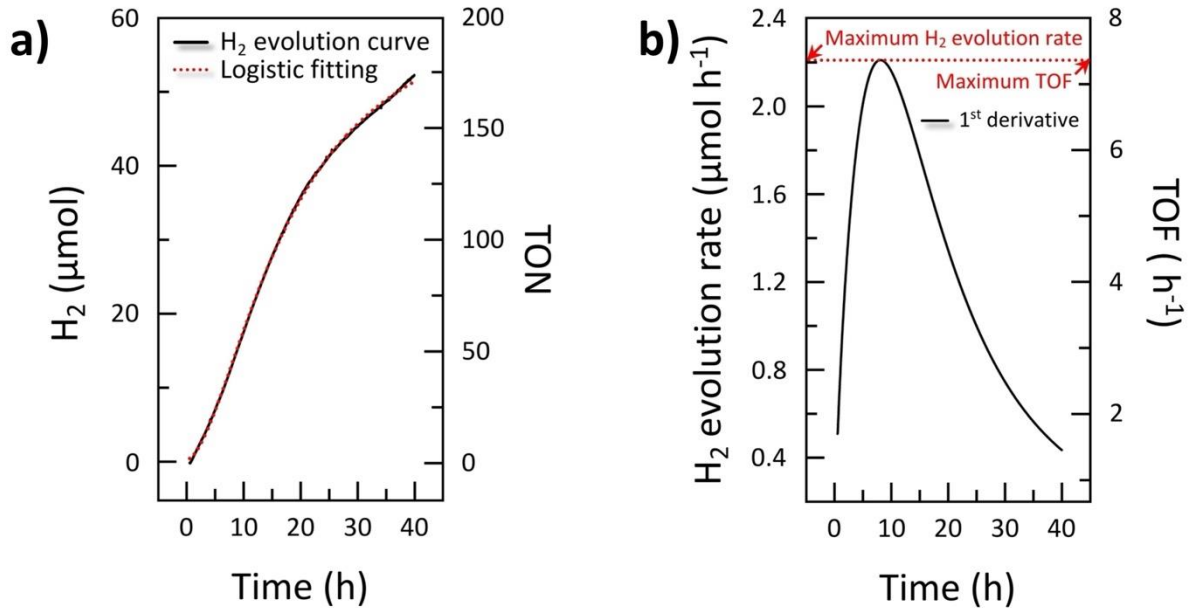

Figure 3.9 *Calculation of maximum O_2 evolution rate and maximum TOF of [Co-OMeP]$^{3-}$.*

3.4.6 Calculation of photochemical H_2 production quantum yield

The H_2 generation quantum yield was calculated using the TOF_{max}, n_{cat} and the rate of photons absorption:

$$\varphi = \frac{2n_{cat}TOF_{max}}{3600\Phi(1-10^{-A_e})(A_{PS}/A_e)}$$

in which TOF_{max} (h^{-1}) is the maximum turnover frequency of the photocatalytic oxygen evolution reaction, n_{cat} (in μmol) is the number of mol of cobalt catalyst used in the photocatalytic experiment, Φ is the photon flux (μmol s^{-1}) determined by standard ferrioxalate actinometry (typically 1.05 μmol s^{-1}, 16 mW),[51] A_e is the total absorption of the photocatalytic solution at 450 nm (A_e>3), A_{PS} is the absorption of photosensitizer only in buffer at 450 nm (A_{PS}/A_e~1), and 3600 is the number of seconds per hour. In this calculation we assumed 2 photons were needed for each molecule of H_2 produced. Errors in triplicate measurements.

3.5 Acknowledgement

C. Liu gratefully acknowledges the China Scholarship Council (CSC) for a personal grant (No. 201706360150).

3.6 References

[1] W. Zhang, W. Lai, R. Cao, *Chem. Rev.* **2017**, *117*, 3717-3797.
[2] P. Du, R. Eisenberg, *Energy Environ. Sci.* **2012**, *5*, 6012-6021.
[3] W. T. Eckenhoff, *Coord. Chem. Rev.* **2018**, *373*, 295-316.
[4] A. Mazzeo, S. Santalla, C. Gaviglio, F. Doctorovich, J. Pellegrino, *Inorganica Chim. Acta* **2021**, *517*, 119950.
[5] H. I. Karunadasa, E. Montalvo, Y. Sun, M. Majda, J. R. Long, C. J. Chang, *Science* **2012**, *335*, 698-702.
[6] B. R. Garrett, S. M. Polen, K. A. Click, M. He, Z. Huang, C. M. Hadad, Y. Wu, *Inorg. Chem.* **2016**, *55*, 3960-3966.
[7] M. Kondo, H. Tatewaki, S. Masaoka, *Chem. Soc. Rev.* **2021**, *50*, 6790-6831.
[8] C. Liu, D. van den Bos, B. den Hartog, D. van der Meij, A. Ramakrishnan, S. Bonnet, *Angew. Chem. Int. Ed.* **2021**, *60*, 13463-13469.
[9] Y. Han, H. Fang, H. Jing, H. Sun, H. Lei, W. Lai, R. Cao, *Angew. Chem. Int. Ed.* **2016**, *55*, 5457-5462.
[10] X. Yang, Z. Hu, Q. Yin, C. Shu, X. F. Jiang, J. Zhang, X. Wang, J. X. Jiang, F. Huang, Y. Cao, *Adv. Funct. Mater.* **2019**, *29*.
[11] H. Lei, C. Liu, Z. Wang, Z. Zhang, M. Zhang, X. Chang, W. Zhang, R. Cao, *ACS Catal.* **2016**, *6*, 6429-6437.
[12] C. Bachmann, B. Probst, M. Guttentag, R. Alberto, *Chem. Commun.* **2014**, *50*, 6737-6739.
[13] B. B. Beyene, C.-H. Hung, *Sustain. Energy Fuels* **2018**, *2*, 2036-2043.
[14] S. Chakraborty, E. H. Edwards, B. Kandemir, K. L. Bren, *Inorg. Chem.* **2019**, *58*, 16402-16410.
[15] F. Gartner, A. Boddien, E. Barsch, K. Fumino, S. Losse, H. Junge, D. Hollmann, A. Bruckner, R. Ludwig, M. Beller, *Chem. Eur. J.* **2011**, *17*, 6425-6436.
[16] E. Giannoudis, E. Benazzi, J. Karlsson, G. Copley, S. Panagiotakis, G. Landrou, P. Angaridis, V. Nikolaou, C. Matthaiaki, G. Charalambidis, E. A. Gibson, A. G. Coutsolelos, *Inorg. Chem.* **2020**, *59*, 1611-1621.
[17] J. G. Kleingardner, B. Kandemir, K. L. Bren, *J. Am. Chem. Soc.* **2014**, *136*, 4-7.
[18] M. P. McLaughlin, T. M. McCormick, R. Eisenberg, P. L. Holland, *Chem. Commun.* **2011**, *47*, 7989-7991.
[19] M. Natali, E. Badetti, E. Deponti, M. Gamberoni, F. A. Scaramuzzo, A. Sartorel, C. Zonta, *Dalton Trans.* **2016**, *45*, 14764-14773.
[20] A. Panagiotopoulos, A. M. Douvas, P. Argitis, A. G. Coutsolelos, *ChemSusChem* **2016**, *9*, 3213-3219.
[21] A. Reynal, E. Pastor, M. A. Gross, S. Selim, E. Reisner, J. R. Durrant, *Chem. Sci.* **2015**, *6*, 4855-4859.
[22] Y. J. Yuan, Z. T. Yu, H. L. Gao, Z. G. Zou, C. Zheng, W. Huang, *Chem. Eur. J.* **2013**, *19*, 6340-6349.
[23] M. Yang, J. E. Yarnell, K. El Roz, F. N. Castellano, *ACS Appl. Energy Mater.* **2020**, *3*, 1842-1853.
[24] Z. T. Yu, X. L. Liu, Y. J. Yuan, Y. H. Li, G. H. Chen, Z. G. Zou, *Dalton Trans.* **2016**, *45*, 17223-17232.
[25] J.-M. Lei, S.-P. Luo, S.-Z. Zhan, *Polyhedron* **2018**, *154*, 295-301.
[26] T. Lazarides, M. Delor, I. V. Sazanovich, T. M. McCormick, I. Georgakaki, G. Charalambidis, J. A. Weinstein, A. G. Coutsolelos, *Chem. Commun.* **2014**, *50*, 521-523.
[27] R. S. Khnayzer, V. S. Thoi, M. Nippe, A. E. King, J. W. Jurss, K. A. El Roz, J. R. Long, C. J. Chang, F. N. Castellano, *Energy Environ. Sci.* **2014**, *7*, 1477-1488.
[28] C. Bachmann, M. Guttentag, B. Spingler, R. Alberto, *Inorg. Chem.* **2013**, *52*, 6055-6061.
[29] M. Natali, *ACS Catal.* **2017**, *7*, 1330-1339.
[30] A. Mahammed, B. Mondal, A. Rana, A. Dey, Z. Gross, *Chem. Commun.* **2014**, *50*, 2725-2727.
[31] M. Vennampalli, G. Liang, L. Katta, C. E. Webster, X. Zhao, *Inorg. Chem.* **2014**, *53*, 10094-10100.
[32] Y. Sun, J. Sun, J. R. Long, P. Yang, C. J. Chang, *Chem. Sci.* **2013**, *4*, 118-124.
[33] A. Panagiotopoulos, K. Ladomenou, D. Sun, V. Artero, A. G. Coutsolelos, *Dalton Trans.* **2016**, *45*, 6732-6738.
[34] K. Ladomenou, M. Natali, E. Iengo, G. Charalampidis, F. Scandola, A. G. Coutsolelos, *Coord. Chem. Rev.* **2015**, *304-305*, 38-54.
[35] B. B. Beyene, S. B. Mane, C. H. Hung, *Chem. Commun.* **2015**, *51*, 15067-15070.
[36] B. C. Martindale, E. Joliat, C. Bachmann, R. Alberto, E. Reisner, *Angew. Chem. Int. Ed.* **2016**, *55*, 9402-9406.
[37] M. F. Zipplies, W. A. Lee, T. M. Bruice, *J. Am. Chem. Soc.* **1986**, *108*, 4433-4445.
[38] S. Nakagaki, F. L. Benedito, F. Wypych, *J. Mol. Catal. A Chem.* **2004**, *217*, 121-131.
[39] J. C. Biffinger, H. Sun, A. P. Nelson, S. G. DiMagno, *Org. Biomol. Chem.* **2003**, *1*, 733-736.
[40] A. R. Parent, K. Sakai, *ChemSusChem* **2014**, *7*, 2070-2080.
[41] T. Nakazono, A. R. Parent, K. Sakai, *Chem. Eur. J.* **2015**, *21*, 6723-6726.
[42] A. Sułek, B. Pucelik, J. Kuncewicz, G. Dubin, J. M. Dąbrowski, *Catalysis Today* **2019**, *335*, 538-549.

[43] T. Nakazono, K. Sakai, *Dalton Trans.* **2016**, *45*, 12649-12652.
[44] L. Troian-Gautier, C. Moucheron, *Molecules* **2014**, *19*, 5028-5087.
[45] D. Paul Rillema, G. Allen, T. J. Meyer, D. Conrad, *J. Am. Chem. Soc.* **1983**, *22*, 1617-1622.
[46] Y. J. Yuan, Z. T. Yu, D. Q. Chen, Z. G. Zou, *Chem. Soc. Rev.* **2017**, *46*, 603-631.
[47] E. Joliat-Wick, N. Weder, D. Klose, C. Bachmann, B. Spingler, B. Probst, R. Alberto, *Inorg. Chem.* **2018**, *57*, 1651-1655.
[48] V. Lyaskovskyy, B. de Bruin, *ACS Catal.* **2012**, *2*, 270-279.
[49] O. R. Luca, R. H. Crabtree, *Chem. Soc. Rev.* **2013**, *42*, 1440-1459.
[50] R. C. J. Murray, P. A. Rock, *Electrochim. Acta* **1968**, *13*, 969-975.
[51] J.G.P. Calvert, J. N., *Chemical actinometer for the determination of ultraviolet light intensities. In Photochemistry.* Wiley and Sons, New York, **1967**, 780.